



Deposited via The University of York.

White Rose Research Online URL for this paper:

<https://eprints.whiterose.ac.uk/id/eprint/95576/>

Version: Accepted Version

Article:

Lee, James D., Helfter, Carole, Purvis, R.uth M. et al. (2015) Measurement of NO_x fluxes from a tall tower in central London, UK and comparison with emissions inventories. *Environmental Science and Technology*. pp. 1025-1034. ISSN: 1520-5851

<https://doi.org/10.1021/es5049072>

Reuse

Items deposited in White Rose Research Online are protected by copyright, with all rights reserved unless indicated otherwise. They may be downloaded and/or printed for private study, or other acts as permitted by national copyright laws. The publisher or other rights holders may allow further reproduction and re-use of the full text version. This is indicated by the licence information on the White Rose Research Online record for the item.

Takedown

If you consider content in White Rose Research Online to be in breach of UK law, please notify us by emailing eprints@whiterose.ac.uk including the URL of the record and the reason for the withdrawal request.

1 Measurement of NO_x fluxes from a tall tower in
2 central London, UK and comparison with
3 emissions inventories.

4
5 *James D. Lee^{*λ§}, Carole Helfter[&], Ruth M. Purvis^{λ§}, Sean D. Beevers[#], David C. Carslaw[#],*
6 *Alastair C. Lewis[§], Sarah J. Moller^{λ§}, Anja Tremper[#], Adam Vaughan^λ, Eiko G. Nemitz[&].*

7
8 [§]National Centre for Atmospheric Science, University of York, York, UK.

9 ^λDepartment of Chemistry, University of York, York, UK

10 [&]Centre for Ecology and Hydrology (Edinburgh Research Station), Penicuik, UK.

11 [#]Environmental Research Group, King's College London, 4th Floor, Franklin Wilkins
12 Building, 150 Stamford Street, London, UK.

13
14
15 **Abstract**

16 Direct measurements of NO_x concentration and flux were made from a tall tower in central
17 London, UK as part of the Clean Air for London (ClearfLo) project. Fast time resolution (10
18 Hz) NO and NO₂ concentrations were measured and combined with fast vertical wind

19 measurements to provide top-down flux estimates using the eddy covariance technique.
20 Measured NO_x fluxes were usually positive and ranged from close to zero at night to 2000 –
21 8000 ng m⁻² s⁻¹ during the day. Peak fluxes were usually observed in the morning, coincident
22 with the maximum traffic flow. Measurements of the NO_x flux have been scaled and
23 compared to the UK National Atmospheric Emissions Inventory (NAEI) estimate of NO_x
24 emission for the measurement footprint. The measurements are on average 80% higher than
25 the NAEI emission inventory for all of London. Observations made in westerly airflow (from
26 parts of London where traffic is a smaller fraction of the NO_x source) showed a better
27 agreement on average with the inventory. The observations suggest that the emissions
28 inventory is poorest at estimating NO_x when traffic is the dominant source, in this case from
29 an Easterly direction from the BT tower. Agreement between the measurements and the
30 London Atmospheric Emissions Inventory (LAEI) are better, due to the more explicit
31 treatment of traffic flow by this more detailed inventory. The flux observations support
32 previous tailpipe observations of higher NO_x emitted from the London vehicle diesel fleet
33 than is represented in the NAEI or predicted for several EURO emission control technologies.
34 Higher than anticipated vehicle NO_x is likely responsible for the significant discrepancies that
35 exist in London between observed NO_x and long-term NO_x projections.

36

37 **Introduction**

38 The oxides of nitrogen NO_x (defined as the sum of NO and NO₂), are emitted as a
39 consequence of most combustion processes. The majority of NO_x is emitted as NO, which is
40 rapidly oxidised to NO₂ upon reaction with ozone (O₃), with the reverse of this process being
41 caused by the action of sunlight on NO₂ to form NO and O₃. NO₂ is known to have
42 significant direct health effects on humans. At high concentrations it causes inflammation of
43 the airways and long-term exposure may affect lung function and enhance the response to

44 allergens^{1, 2}. In addition, NO_x contributes to the formation of O₃ and secondary particles
45 through a series of photochemical reactions³. As a result of this, NO₂ is included in a series
46 of air pollutants identified as part of the EU Air Quality Directive (AQD, 2008)⁴ which sets
47 limit values for hourly and annual mean exposure. It has been shown by measurements and
48 models that the annual mean limit value of 40 µg m⁻³ continues to be exceeded in many urban
49 centres throughout the UK⁵, including London. Measures are in place to control the
50 emissions of nitrogen oxides and UK emissions are projected to decline by about 35 %
51 between 2010 and 2020⁶. However, it is known that ambient NO₂ concentrations do not
52 respond linearly to reductions in the concentration of NO_x (e.g. Derwent et al., 1995⁷), mainly
53 because of the chemical coupling of ozone (O₃) and NO_x under ambient conditions⁸. In
54 addition, changes in diesel emission control technology have led to increases in directly
55 emitted NO₂⁹. Trends in ambient concentrations of NO_x and NO₂ in the UK have generally
56 shown a decrease in concentration from 1996 to 2002, followed by a period of more stable
57 concentrations from 2004–2012¹⁰. This is not in line with the expected decrease suggested
58 by the UK emission factors¹¹.

59 Air pollutant emission inventories provide input data for air pollution models, which in turn
60 are used for predicting current and future air pollution. This is typically done using a ‘bottom
61 up’ approach involving estimated emissions from different source sectors to produce yearly
62 emission estimates. However it is known that this method can contain large uncertainties,
63 with the errors propagating through into errors in air pollution models¹². Evaluation of
64 emission inventories can be carried out by comparing air quality model predictions (using
65 inputs from the inventory) to observed concentrations^{13, 14}, however this method does not
66 provide a direct comparison with the emission rate as it requires knowledge of other
67 parameters such as chemistry and meteorology. The eddy covariance technique provides a
68 direct measurement of the flux to the atmosphere of a particular pollutant, thus providing a

69 ‘top down’ approach to quantifying emissions¹⁵. Flux measurements also provide
70 information on both spatial and temporal change in emissions from a calculated flux
71 footprint, giving insight into controls and sources. The majority of eddy covariance
72 measurements made to date have concentrated on fluxes of greenhouse gases (CO₂, CH₄ and
73 N₂O)^{16, 17} and volatile organic compounds (VOCs)¹⁸⁻²⁰, largely from biogenic sources. Some
74 eddy covariance NO_x flux measurements have been made and have typically focused on
75 emissions from soils²¹, forests²²⁻²⁴ or snow^{25, 26}. Recently however, it has been shown that
76 this method can be extended to the urban canopy for CO₂²⁷⁻²⁹ and VOCs³⁰⁻³², with one study
77 of urban NO_x³³.

78 In this study, we use the eddy covariance technique to directly measure the flux of NO and
79 NO₂ from a tall tower (190 m) in central London as part of the Clean Air for London
80 (ClearfLo) project³⁴. The results are compared to local traffic flow and a flux footprint is
81 calculated to allow comparison with two emission inventories, one for the whole of the UK
82 and one specific to London.

83

84

85 **Experimental**

86 *Measurement site*

87 Measurements were made during June – August 2012 and March – April 2013 from the top
88 of the BT tower, a 190m tall telecommunications tower situated in central London, UK
89 (51°31’17.4’’N 0°8’20.04’’W). Mean building height is 8.8 ± 3.0 m within 1 - 10 km of the
90 tower and 5.6 ± 1.8 m for suburban London beyond this^{30, 35}. The area surrounding the tower
91 is dominated by roads and commercial / residential buildings, but also includes some urban
92 parkland and pervious ground. A map of the location of the tower within London is shown in
93 the supplementary information (Figure S1). The gas inlet and ultrasonic anemometer were

94 attached to a mast which extended ~3 m above the top of the tower. Air was pumped down a
95 ~40 m long Teflon tube (1/2" OD) at a flow rate of ~30 L min⁻¹ to the gas instruments which
96 were housed in a room inside the tower.

97 The most prevalent wind direction during the summer 2012 measurement period was the
98 SW sector (~50 % of the time), with other wind sectors split approximately equally. Wind
99 speed was 6.7 ms⁻¹ on average, with the highest wind speeds measured when the wind was
100 from a NW direction. Average temperature was 15.1 ± 4.3 °C. During the March and April
101 2013 measurement period, the most prevalent wind direction was between 0 - 90° (50 %),
102 again with other directions split approximately equally. Wind speed was higher than summer
103 2012, being 8.8 m s⁻¹ on average with the highest wind speed when the wind was from the
104 SW direction. As expected, average temperature was lower than the summer 2012 period,
105 being 9.7 ± 2.4°C.

106

107 *NO_x measurements*

108 Measurements of NO were made using an Ecophysics 780TR instrument, which uses the
109 chemiluminescence technique^{36, 37}. NO₂ was quantified in a second identical NO instrument
110 by initial photolytic conversion to NO using blue light LED diodes centred at 395 nm. The
111 395 nm wavelength has a specific affinity for NO₂ photolytic conversion to NO, giving high
112 analyte selectivity within the channel³⁸ and there is a low probability of other species such as
113 nitrous acid (HONO) being photolysed. The diode based converter also has a very low
114 residence time for the air sample (< 0.1s) which allows 10 Hz measurements of NO₂ to be
115 made. The NO instruments were calibrated every 36 hours by addition of a known amount of
116 NO to the sample line, made by diluting a gas standard (5 ppm NO in N₂, BOC – traceable to
117 NPL scale) in NO_x free air (Ecophysics PAG003). The conversion efficiency of the NO₂
118 converter was also measured during each calibration by gas phase titration of the known NO

119 upon addition of O₃, with typical conversion efficiencies being 30 - 35%. It is estimated that
120 the total error (including accuracy and precision) is around 10 % for NO and 15 % for NO₂ at
121 10 ppbv.

122

123 *Meteorology measurements*

124 Fast (20 Hz), 3 dimensional wind vectors and sonic temperature were measured from next
125 to the sample line inlet by a Gill Instruments R3-50 ultrasonic anemometer. The data was
126 logged, along with that from the NO_x instrument, using a custom National Instruments
127 LabViewTM program. The boundary layer height was measured using a HALO Photonic
128 Doppler LiDAR instrument³⁹.

129

130 *Flux calculations and uncertainties*

131 NO and NO₂ fluxes (F_{NO} and F_{NO₂}) were calculated using eq. 1 and 2 below.

$$132 \quad F_{NO} = \frac{\overline{w' C'_{NO}}}{S_{NO} V_{mol}} \quad (1)$$

133

$$134 \quad F_{NO_2} = \frac{1}{\alpha V_{mol}} \left\{ \frac{\overline{w' C'_{NO_2}}}{S_{NO_2}} - \frac{\overline{w' C'_{NO}}}{S_{NO}} \right\} \quad (2)$$

135

136 C_i is the number of instrument counts (in Hz) and S_i is the associated instrument sensitivity
137 (in Hz ppb⁻¹) for species i (NO and NO₂). V_{mol} is the molar volume (calculated for each
138 individual point), α is the photolytic conversion efficiency of NO₂ to NO and w is the vertical
139 wind component measured by the ultrasonic anemometer. A “prime” symbol represents an
140 instantaneous deviation from the mean and a horizontal bar denotes the covariance of 2
141 scalars.

142 Processed data were filtered using a three-step quality assurance algorithm whereby data
143 were deemed of satisfactory quality if:

144 The level of turbulence was sufficient, i.e. locally-derived friction velocity $u_* \geq 0.2 \text{ m s}^{-1}$
145 (<5% of the data is rejected due to this parameter)

146 The number of spikes in w , NO and NO_2 did not exceed 1% of total in each half-hourly
147 averaging period.

148 The stationarity test described by Foken et al.^{40, 41}, which requires the flux for the complete
149 averaging interval (here 30 min) to be within 30 % of the fluxes calculated for the sub-
150 intervals (6×5 minutes), was satisfied.

151 Total measurement uncertainty, i.e. the sum of total random and systematic uncertainties,
152 was estimated using the 24-hour differencing method⁴² whose assumption is that the
153 difference between pairs of observations taken exactly 24 hours apart under similar
154 meteorological conditions (air temperature, wind speed and direction) is mainly attributable
155 to stochastic factors. Using multiple pairs of observations, the standard deviation of the
156 random error can be calculated from eq. (3).

$$157 \quad \sigma = \frac{\sigma(x_{1,t} - x_{2,t})}{\sqrt{2}} \quad (3)$$

158

159 The environmental conditions were deemed similar if:

160 Air temperatures diverged by less than 3 °C.

161 Wind speed diverged by less than 2 m s⁻¹.

162 Wind directions originated from the same quadrant.

163

164 Causes of systematic uncertainties are varied and include calibration procedures,
165 instrumentation limitations or data processing artefacts. Unlike random uncertainties,
166 systematic errors can be minimized by careful data processing and correction.

167 Successive calibration events were linearly interpolated over time cancelling out errors due
168 to calibration drifts provided that the drift is linear over time.

169 To estimate potential turbulence attenuation in the sampling line, which can lead to
170 underestimation of the actual flux, fluxes of CO₂ measured using by a Picarro G2301-f
171 sampling off the same line as the NO and NO₂ analysers were compared with fluxes
172 measured by a Licor 7500 open-path analyser mounted near the ultrasonic anemometer. The
173 underlying assumption is that turbulence attenuation and molecular interactions with the
174 sampling tube are comparable for CO₂, NO and NO₂ molecules. Rather than correct for
175 attenuation, this systematic uncertainty was added to the estimated stochastic component and
176 presented as confidence interval in what follows.

177

178 *Flux footprint*

179 In order to carry out meaningful interpretation of the data, it is necessary to calculate the
180 flux footprint of the measurement. It is not possible to get footprint models to fully account
181 for the spatial variability of building heights, topography and surface heat flux from an urban
182 environment. In this case, the Kormann and Meixner (2001)⁴³ footprint model (K-M model)
183 was applied, which accounts for non-neutral stratification but assumes homogeneous
184 surfaces. The aerodynamic roughness length for momentum was assumed to be 1 m as used
185 in previous BT Tower flux studies³⁵. The sample height for the BT Tower was 190 m. The K
186 - M model was used to estimate the flux footprint on a half hourly time base. A Microsoft
187 Excel tool (based on the K - M model) calculates the distance from the measurement point at
188 which a set percentage of the measured flux is emitted from. Figure S4 in the supplementary
189 information shows a histogram of the calculated footprints for 50 %, 70 % and 90 % of the
190 flux for the measurement period. The analysis here uses the footprint where 90 % of the flux

191 is predicted to originate from, which shows a range of 150 m – 19980 m with a median of
192 4695 m.

193

194 **Results and discussion**

195 Measurements of the NO_x flux were made during two time periods, June – August 2012
196 (36 days) and March – April 2013 (28 days). Downtime was due mainly to instrument failure
197 of both the fast NO_x instrument and 3-D sonic anemometer, as well as a failure in the sample
198 pump. Despite this, data coverage on the days when measurements was taken (61 %),
199 meaning the dataset provides a unique opportunity to examine the diurnal and seasonal
200 behavior of NO_x fluxes from central London.

201 The full time series of data is shown in the supplementary information Figure S2, with NO_x
202 concentrations averaged to the 30 minute flux averaging time. Typically NO concentrations
203 vary from close to zero at night to a maximum of 10 – 100 µg m⁻³ during the day, whereas
204 NO₂ ranges from 5 – 80 µg m⁻³. Also shown in Figure S2 is the time series of NO and NO₂
205 from an urban background site in at North Kensington, London, which is approximately 5 km
206 west of the BT tower⁴⁴. These data show similar trend to the BT tower for most of the time,
207 although at generally higher levels. A regression analysis of the two datasets (BT tower and
208 North Kensington, shown in supplementary information Figure S3), shows North Kensington
209 data being on average 10 % higher for NO and 6 % higher for total NO_x (R² of 0.65 and 0.58
210 respectively). This result gives confidence that, at least for total NO_x, the BT tower site is
211 representative of the wider London area.

212 Random uncertainties (1 σ) obtained by 24-hour differencing were 441 ng m⁻² s⁻¹ for F_{NO},
213 475 ng m⁻² s⁻¹ for F_{NO₂} and 510 ng m⁻² s⁻¹ for F_{NO_x} (F_{NO} + F_{NO₂}); residual systematic
214 uncertainties, were estimated at 15% of the measured flux. Maximum NO_x fluxes are
215 measured during the daytime, with values from 2000 ± 741 to 5000 ± 1191 ng m⁻² s⁻¹ for NO

216 and 2000 ± 775 to 12000 ± 2275 $\text{ng m}^{-2} \text{s}^{-1}$ for NO_2 . Measured fluxes are usually positive,
217 demonstrating, as expected, that NO_x emission dominates over deposition in this urban
218 environment and that it is likely to be dominated by anthropogenic emissions. NO_x can be
219 lost to the surface by dry deposition⁴⁵, and assuming a deposition velocity of 0.1 cm^{-1} and a
220 NO_x concentration of $50 \mu\text{g m}^{-3}$, then the downward flux can be estimated to be in the region
221 of $100 \text{ ng m}^{-2} \text{s}^{-1}$, which is more than an order of magnitude smaller than the observed values.
222 NO and NO_2 fluxes show a distinct diurnal profile. NO flux is close to zero at night (although
223 still positive), with a rise starting at 05:00 to a peak of $1800 - 1900 \text{ ng m}^{-2} \text{s}^{-1}$ between 08:00
224 and 12:00. The NO flux then usually starts to decrease throughout the rest of the day and into
225 the night, reaching the nighttime value of $100 - 200 \text{ ng m}^{-2} \text{s}^{-1}$ at around 20:00. NO_2 flux also
226 typically shows a diurnal profile with $500 - 1000 \text{ ng m}^{-2} \text{s}^{-1}$ measured at night followed by a
227 rise to $2200 - 2300 \text{ ng m}^{-2} \text{s}^{-1}$ from 05:00 until 12:00, with levels then remaining constant
228 until around 16:00. There follows a steady decrease in NO_2 flux throughout the rest of the
229 day and into the night, with levels reaching around $1200 \text{ ng m}^{-2} \text{s}^{-1}$ at midnight.

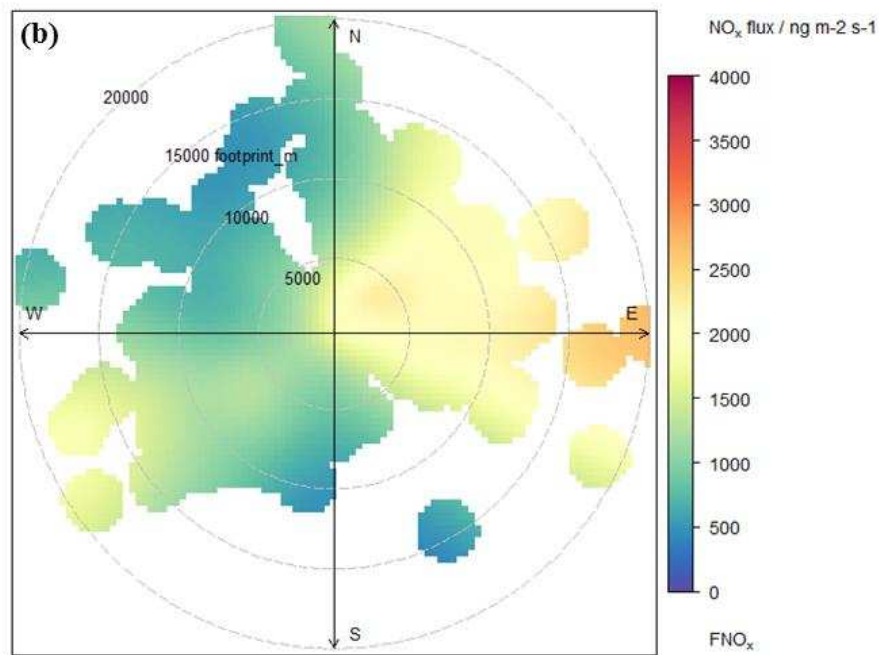
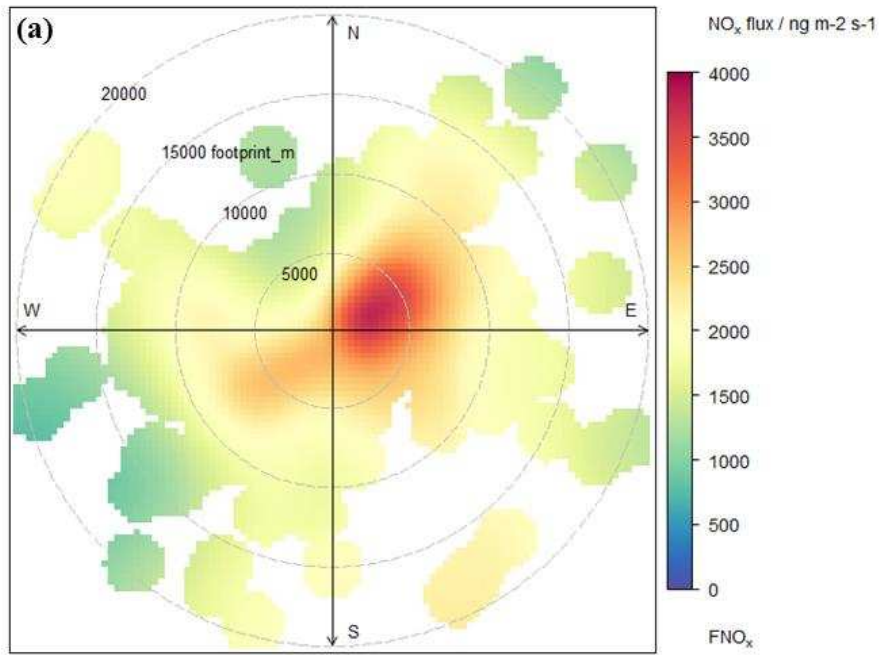
230 Very few direct flux measurements of NO and NO_2 have been made in an urban
231 environment, however the values measured in this study are comparable to a study in the
232 urban area of Norfolk, Virginia, USA, which reported total NO_x fluxes in the range $5000 -$
233 $8000 \text{ ng m}^{-2} \text{s}^{-1}$ ³³. Direct measurements of NO_x fluxes have been made previously over
234 forested and snow pack environments, with the measured fluxes still positive, but typically an
235 order of magnitude smaller than measured here^{22, 24, 25}. Because of the close coupling of NO
236 and NO_2 , it is the sum NO_x that is typically reported in emission inventories, and so the rest
237 of this work will concentrate on measurements of total NO_x . This also allows us to discount
238 the chemistry associated with the inter-conversion of NO and NO_2 , which can happen on a
239 very fast timescale., Total NO_x is likely to be conserved between emission and sampling on
240 the BT tower, as formation of NO_x reservoir species such as PAN and HNO_3 takes place on a

241 much longer timescale than the time between emission from street level and sampling at the
242 tower (estimated as 3 – 8 minutes).

243 Analysis of the wind sector dependence of the flux can help to identify the sources of the
244 species in question. Figure 1 shows bivariate polar plots with the joint flux footprint-wind
245 direction of the NO_x flux, created using the Openair package⁴⁶. The flux footprint used was
246 calculated using the method described above. Two plots are shown to reflect daytime (05:00
247 – 19:00) and night time fluxes. During the daytime, there are clearly higher fluxes measured
248 when the calculated footprint is smaller, in particular when the wind is from an E / NE
249 direction from the tower. Fluxes then get smaller as the footprint gets larger in all directions.
250 This is a reflection of the reduced traffic density (and hence traffic emissions), further away
251 from central London. At night the fluxes are lower in all directions and for all footprints (as
252 expected), however there is much less of a reduction in flux as the footprint gets larger. An
253 explanation for this behavior is likely that traffic emissions are much less important for the
254 total night time NO_x emission, with the majority of the emissions from commercial, industrial
255 and domestic combustion. Hence there is more homogeneity over London during the night
256 compared to the daytime. There are still greater fluxes measured when the wind was from
257 the NE – SE sector, which is probably due to the area to the east of the tower being more
258 urban in nature than that to the west.

259

260



261

262

263 **Figure 1.** Wind sector dependence of the NO_x flux for all data averaged during (a) daytime

264 (05:00 – 19:00) and (b) nighttime (20:00 – 04:00). The radial axis shows the calculated flux

265 footprint in metres for each measurement.

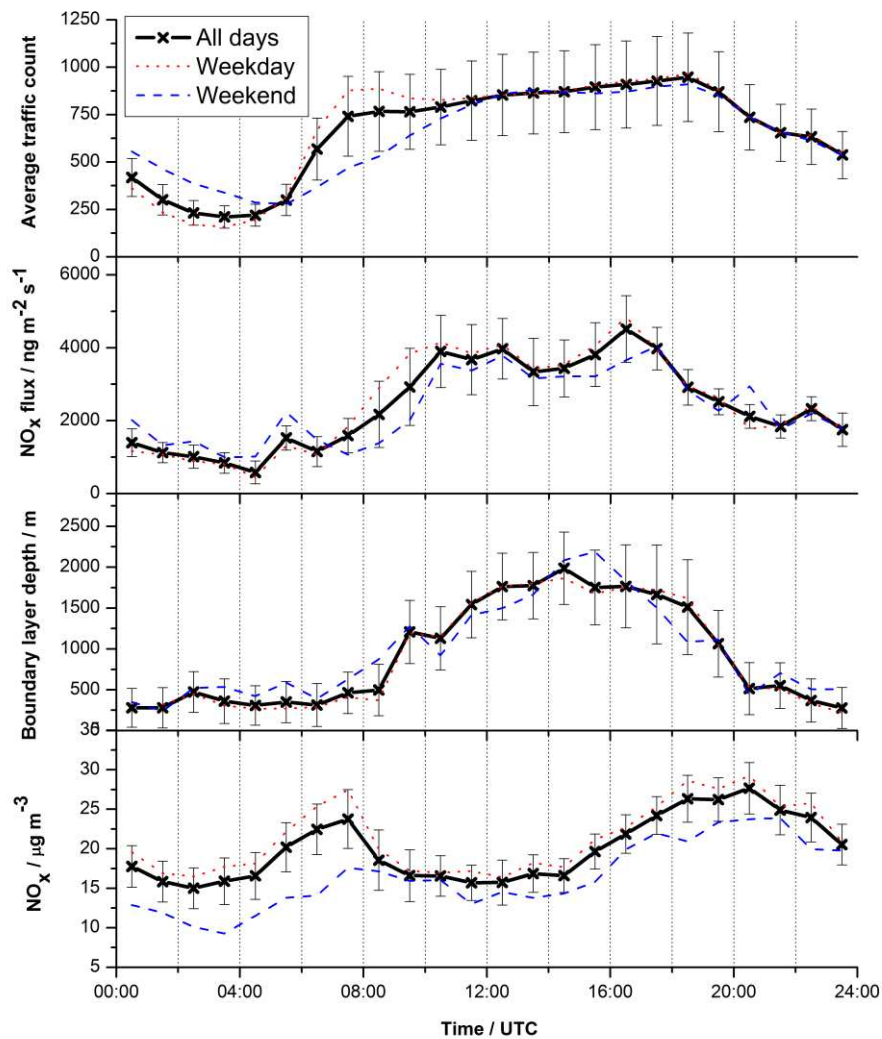
266

267

268 Concentrations of a given pollutant in the atmosphere are largely dependent on its emission
269 rate, meteorology and chemical processing. It is useful to consider diurnal profiles in all these
270 quantities because it can help understand the processes leading to what is observed. For
271 diurnal averages, systematic uncertainties greatly outweigh random uncertainties which
272 decrease as $1/\sqrt{n}$, with n the sample size. Average diurnal cycles have been calculated for
273 the entire measurement period, for NO_x flux, average traffic volume at 20 traffic counting
274 sites within the flux footprint of the site, boundary layer height and NO_x concentration and
275 this data is shown in Figure 2 (all times local time). Standard deviations of the average
276 diurnals are also shown, demonstrating the relatively small day to day variability of the
277 measurements. The traffic data used can be thought of as a proxy for total traffic flow across
278 the entire flux footprint area and a map of the location of the traffic counting sites used is
279 shown in the supplementary information (Figure S5). Data from each day is binned into
280 hourly time periods (UTC = local time -1 hour) and averaged, with the time stamp being the
281 mid-time of the averaging period. NO_x flux shows a diurnal cycle with positive fluxes seen
282 throughout the day. From 00:00 to 04:00 fluxes are slightly decreasing from 1400 ± 210 ng
283 $\text{m}^{-2} \text{s}^{-1}$ to 450 ± 67 ng $\text{m}^{-2} \text{s}^{-1}$, with a rise starting at around 04:30, consistent with the onset of
284 the morning rush hour in London (at 05:30 local time). There follows a steady increase in the
285 NO_x flux to around 4000 ± 600 ng $\text{m}^{-2} \text{s}^{-1}$ at 10:00, levels that remain until 17:00 (with a
286 slight second peak at 16:00). This is broadly similar to the average traffic count data,
287 providing more evidence that the majority of the NO_x emissions sampled at the BT tower are
288 from road traffic emissions. There then follows a steady decrease in the NO_x flux throughout
289 the rest of the day, to around 1200 ± 180 ng $\text{m}^{-2} \text{s}^{-1}$ at 00:00. This is again broadly in line with
290 the traffic flow. NO_x concentrations are reasonably stable at $\sim 18 - 20$ $\mu\text{g m}^{-3}$ throughout the
291 night, followed by a rapid rise starting at 04:30 (at similar time to the rise in NO_x flux). This

292 rapid rise is due to a combination of the increase in fluxes, and the fact that the boundary
293 layer height does not increase until around 06:30. Once the boundary layer starts to grow
294 (from ~ 300 m at 08:00 to 1700 m at 12:00), the rise in NO_x concentrations is less rapid, and
295 in fact they start to fall after a peak of 22 µg m⁻³ at 08:00 until 16:00. This is likely due to
296 dilution effects caused by the increasing height of the boundary layer meaning the NO_x is
297 emitted into a larger volume. After 15:30, the NO_x concentrations start to rise again, despite a
298 decrease in flux. This is again likely due to the meteorology, with a decreasing boundary
299 layer height into the night.

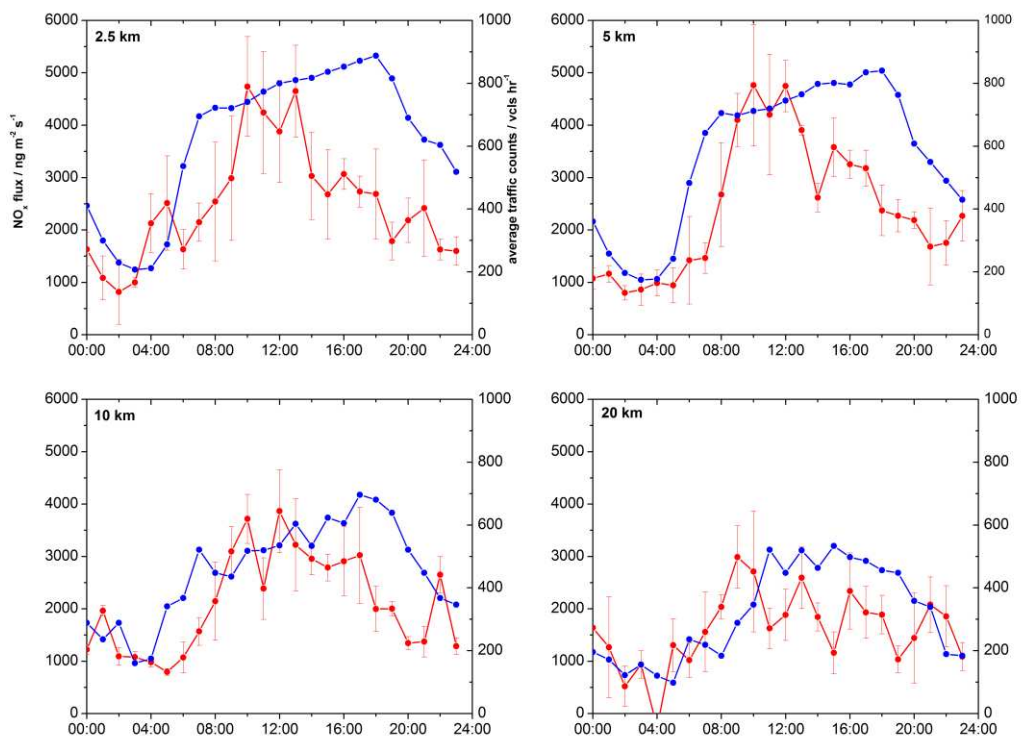
300 Also, plotted in Figure 2 is the weekday and weekend diurnal average for the data. During
301 the day, traffic counts are on average lower during the weekend, particularly during the
302 morning where the difference is up to 50 %. This is reflected in the NO_x flux data, although it
303 does not show as pronounced a difference between weekend and weekday. This is potentially
304 due to the type of traffic at the weekend, which is likely to be predominantly buses and larger
305 vehicles (mainly powered by diesel engines), whereas during the week, private cars and taxis
306 maybe more prevalent. During the night, traffic levels are actually higher at the weekend
307 than during the day, also likely to be a result of public transport and the large nighttime
308 weekend economy of London. This is also reflected in the NO_x flux measurements showing
309 higher values from midnight to 06:30 for weekends compared to weekdays.



310

311 **Figure 2.** Average diurnal profiles for 36 days of data during Jun – Aug 2012 and 28 days
 312 during March and April 2013. Data shown are average traffic count (see text for further
 313 details), NO_x flux, boundary layer depth and NO_x mass mixing ratio. All times local time
 314 with the time stamp the mid-point of an hour averaging period. Error bars reflect the 95 %
 315 confidence intervals in the mean of the different measurements used to calculate the diurnal
 316 average. The red dotted line shows weekday data and the blue dashed line show weekend
 317 data.

318 The flux data was binned into 4 different regimes according to the calculated footprint (0 -
319 2.5, > 2.5 - 5, > 5 - 10 and > 10 - 20 km radial distance from the BT tower) and average
320 diurnal profiles for each are plotted in Figure 3. The shaded regions represent the 95 %
321 confidence of the day to day variability of the flux measurements. All regimes show a
322 similar diurnal profile, with the flux starting to rise at around 04:30, with a peak between
323 10:00 and 14:00. The highest fluxes are seen in the two smallest footprint regimes, with both
324 showing similar values during daytime of around $4500 \pm 675 \text{ ng m}^{-2} \text{ s}^{-1}$. The 5 - 10 km
325 regime shows lower daytime peak fluxes of $3200 \pm 480 \text{ ng m}^{-2} \text{ s}^{-1}$, with the 10 - 20 km
326 regime lower still, with a peak of $2950 \pm 442 \text{ ng m}^{-2} \text{ s}^{-1}$ at 10:00 and then a decline
327 throughout the day. All 4 regimes show similar NO_x fluxes at night of around $1000 \pm 150 \text{ ng}$
328 $\text{m}^{-2} \text{ s}^{-1}$, the exception being the 0 - 2.5 km, which does exhibit some elevated flux levels up to
329 $1500 \text{ ng m}^{-2} \text{ s}^{-1}$, and appears to start to rise slightly earlier than the other regimes. All this
330 behavior is consistent with traffic emissions being the dominant source of NO_x , especially in
331 central London. It is expected that traffic volume will be higher closer to central London and
332 this is shown by the average traffic counts also plotted in the different footprint bins in figure
333 4. As a result of this, the smaller footprint regimes from the BT tower show the largest
334 daytime fluxes. At night, it is likely that a smaller proportion of the NO_x will come from
335 traffic sources, meaning the measured flux will be similar in all flux regimes out to 20 km
336 from the measurements site.
337



338

339 **Figure 3.** Average diurnal profiles for NO_x flux in 4 different footprint regimes (red trace).

340 The error bars reflect the 95 % confidence intervals in the mean of the different

341 measurements used to calculate the diurnal average. All times local time with the time stamp

342 the mid-point of an hourly averaging period. Also shown is the average traffic flow at 6 sites

343 within each of the individual footprint areas (blue trace).

344 *Emissions inventories*

345 In order to put the measured data in some context, a comparison has been carried out

346 against inventories of NO_x emissions for London. The UK National Atmospheric Emissions

347 Inventory (NAEI) shows official annual, spatially disaggregated 1 x 1 km gridded emission

348 maps for a wide range of atmospheric pollutants, including NO_x. A detailed description on

349 how the emissions maps are produced is given in Bush et al. 2008⁴⁷. Briefly, annual emission

350 estimates are generated from 11 source sectors, according to those laid out by the United

351 Nations Economic Commission for Europe (UNECE). For each sector a national total
352 emission estimate is produced from a combination of reported emissions and estimates based
353 on modelling. The UK National Atmospheric Emission Inventory (NAEI) gives an estimate
354 of the NO_x emissions in 1 km² grids over the UK, including a breakdown of the different
355 sources. The NAEI estimate for NO_x emissions for London is shown in the supplementary
356 information (Figure S6). The map is centered on the BT tower and features of London
357 characterized by large NO_x emissions can clearly be seen (e.g. Heathrow airport to the West
358 and the M25 orbital motorway circling the city). Four maps are shown, with the contribution
359 from 3 of the most important sectors (road transport, domestic, industrial and commercial
360 combustion and other transport (rail and shipping), as well as the total emissions. Also shown
361 on the maps are 5 km and 10 km radius circles from the tower, indicative of the flux footprint
362 bins described above. It suggests that around 65 % of NO_x emissions from central London are
363 from road and other transport, with the majority of the remainder from commercial, domestic
364 and industrial combustion.

365 The London Atmospheric Emissions Inventory (LAEI) provides emissions estimates of 9
366 air pollutants (including NO_x), on a 20 m x 20 m grid square scale. The inventory reflects the
367 geography of the roads in London, enabling an accurate assessment of population exposure
368 and health impacts. Two versions of the LAEI are used in this study. The standard LAEI
369 (LAEI base) is the 2012 inventory based on methods set out in the Greater London Authority
370 datastore⁴⁸, but updated for 2012 emission data. Also, we use an enhanced version of the
371 LAEI, which uses measured roadside emissions based on extensive vehicle emission remote
372 sensing⁴⁹. Both emissions inventories discussed are purely annual averages with no seasonal
373 or finer temporal detail.

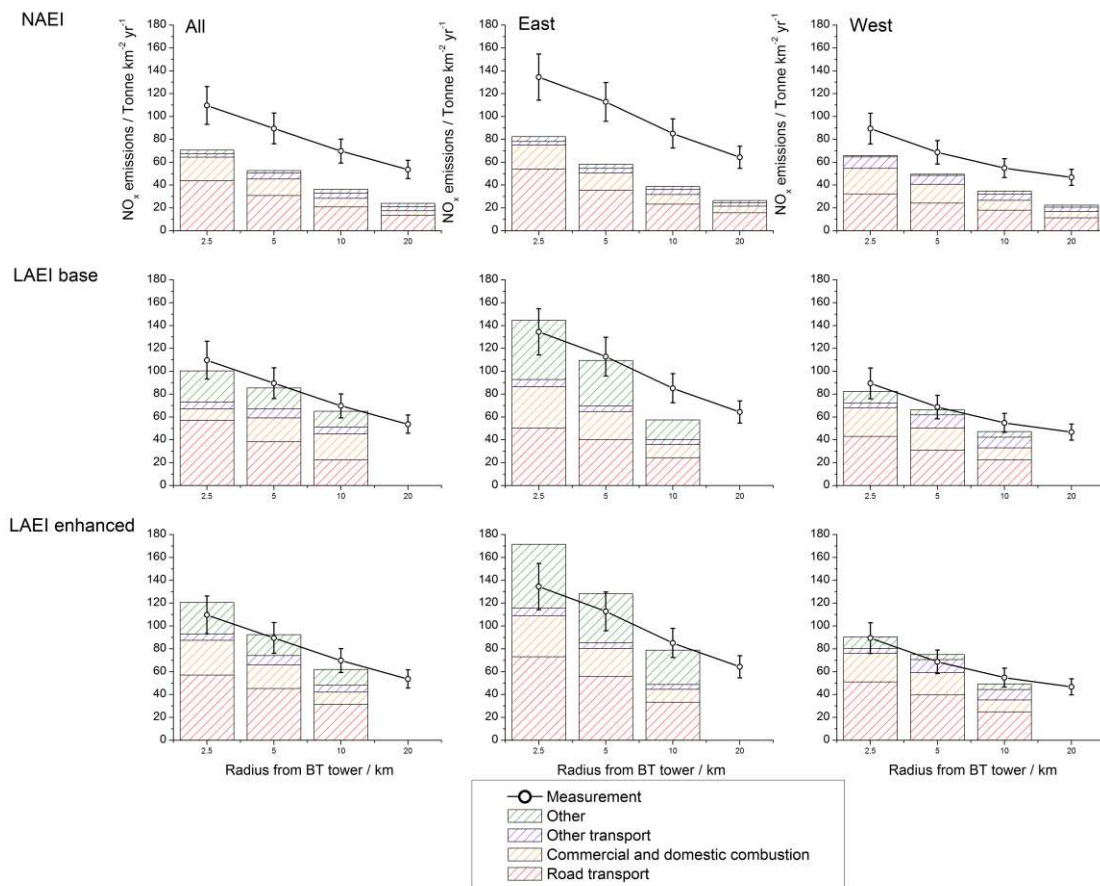
374

375

376

377 *Comparison with measurements*

378



379

380 **Figure 4.** Comparison of the averaged measured fluxes, scaled to give an annual emission
381 rate, with the estimate of the National Atmospheric Emission Inventory (NAEI) and two
382 versions of the London Atmospheric Emissions Inventory (LAEI) – see text for details. The
383 different colours in the columns represent the estimates from different source sectors.

384

385

386 Figure 4 shows estimated emissions of NO_x taken from the NAEI and LAEI for 2.5 km, 5
387 km and 10 km radial distance from the tower, along with the estimates for sections in easterly

388 (30 – 150°) and westerly (210 – 330°) directions and the source sector estimate divided into
389 road transport, commercial and residential combustion and other transport (which is mainly
390 rail in London). For the NAEI data for a 20 km radial distance is also plotted however this
391 data is not available for the LAEI. Also plotted is the averaged measured NO_x flux for the
392 different footprint regimes, also divided into periods of easterly and westerly wind directions
393 and scaled to give a yearly emission rate.

394 The measurements are seen to be significantly higher than the NAEI (outside the estimated
395 experimental flux systematic error of 15 %) under all regimes. The agreement between the
396 measurement and the inventory tends to get worse for the larger footprint regimes, with the
397 measurement being 2.2 times higher than the inventory for the 10 – 20 km regime, and only
398 1.6 times higher for the 0 – 2.5 km regime. There is much more scope for error when
399 considering a comparison between larger flux footprints and the inventory as the further the
400 air has travelled, the more different emission inventory grid squares it could have passed
401 over, making a comparison with the inventory more difficult. In general the agreement is
402 better for the westerly flow conditions, with the measurement being 1.36 and 1.38 times
403 higher than the inventory for the 2.5 km and 5 km footprints respectively, whereas for the
404 easterly flow, the agreement is worse (1.6 and 1.9 times higher for 2.5 km and 5 km). The
405 difference in source sector between the 2.5 km and 5 km radius is small. Road transport
406 dominates (62 % and 60% for 2.5 km and 5 km respectively), with the remainder from
407 commercial and domestic combustion (29 % and 27 %) and other transport (4 % and 10 %).
408 There is a lower contribution from road transport for the westerly flow conditions (48 % for
409 both 2.5 km and 5 km radius), giving a potential reason for the better agreement here. It is
410 likely that road transport is the most poorly constrained part of the NAEI, and hence when
411 this is less important to the total emission rate, the agreement with the measurement is better.

412 For the base LAEI, the comparison shows a much closer agreement of the measurements
413 with the inventory compared to that with the NAEI discussed above. The inventory is within
414 the measurement error for the average of all wind directions, with the measurement 1.03 and
415 1.1 times higher than the inventory in the 2.5 km and 5 km regimes respectively. The
416 agreement is similarly good in westerly flow, and although in Easterly flow the measurement
417 is now 1.07 times lower for the 2.5 km footprint and 1.03 times higher for the 5 km footprint,
418 these are still well within measurement error. For the 10 km footprint, the LAEI falls outside
419 the systematic error of the measurements for all the data separated into easterly and westerly
420 flow regimes, the measurements being 1.16 and 1.48 times higher than the inventory for
421 westerly and easterly flow respectively. A comparison of the measurements to the enhanced
422 LAEI (which has generally increased road transport NO_x emissions), shows the
423 measurements being slightly lower than the inventory for data from the 2.5 km and 5 km flux
424 footprints, although again these is still within the systematic error of the measurements for all
425 the data and the westerly flow. It is in the easterly flow conditions where the measurements
426 are now significantly lower than the inventory, with the underestimation of 20 % and 17 %
427 for the 2.5 km and 5 km regimes falling outside the flux measurement error. For the 10 km
428 flux footprint regime, the enhanced LAEI brings the emission estimates into much better
429 agreement with the measurements than the base case, with the data from both easterly and
430 westerly flows showing agreement within 10 %.

431 In general both the LAEIs seem to be doing a reasonable job of estimating NO_x emissions
432 in central London, and certainly better than the NAEI estimations. The LAEI, particularly in
433 its enhanced form with measured road traffic emissions, has a much more explicit treatment
434 of road transport emission than the NAEI, thus potentially providing a more accurate estimate
435 of NO_x emissions in London. It uses vehicle speed and vehicle flow data from each road link
436 using GPS based vehicle speed, as well as automatic number plate recognition data to

437 enhance vehicle stock information. The inventory also makes predictions of primary NO₂
438 emissions, something that is potentially important in London due to the high proportion of
439 diesel fuelled vehicles, which are likely to have a higher direct primary NO₂ emission
440 compared to petrol vehicles⁵⁰. The LAEI containing the enhanced treatment of traffic
441 emissions actually overestimates the NO_x emission in the central London footprint regimes (0
442 - 5 km from the BT tower), with greater overestimation outside the error of the measurements
443 under easterly flow conditions. This suggests potential extra errors in the treatment of traffic
444 flow in the center of London to the east of the BT tower within the LAEI. The LAEI has a
445 significant contribution from other sources, which are mainly from non-road mobile
446 machinery (e.g. cranes, construction vehicles). These are virtually zero in the NAEI and it
447 could be errors in these sources that are contributing to the overestimation of the inventory in
448 central London. The better comparison with the LAEI compared to the NAEI support
449 previous tailpipe observations of higher NO_x emitted from the London vehicle diesel fleet
450 than is represented in the NAEI or predicted for several EURO emission control technologies
451 and show that a detailed treatment of traffic emissions is required to properly predict the NO_x
452 emissions¹¹. There are no studies to our knowledge that specifically evaluate the London or
453 national inventories. However, it is clear from recent remote sensing measurements in
454 London during 2012 that emissions of NO_x have not decreased as expected through emissions
455 legislation⁴⁹. This higher than anticipated vehicle NO_x is likely responsible for the significant
456 discrepancies that exist in London between observed NO_x and long-term NO_x projections,
457 and show that a detailed representation of traffic emissions is required to accurately represent
458 NO_x in London.

459

460

461 **Associated content**

462 *Supporting information*

463 Figures S1 – S6 show a location map of the site, the time series of NO_x levels and fluxes
464 from the BT tower, regression between BT tower NO_x and NO_x measured at a nearby urban
465 background site, flux footprint statistics, a map of the location of the traffic count sites and
466 maps of the 1km x 1km National Atmospheric Emission Inventory (NAEI) source specific
467 emissions for NO_x. This information is available free of charge via the Internet at
468 <http://pubs.acs.org/>

469

470

471 **Author information**

472 *Corresponding Author*

473 Phone: +44 (0)1904 322575, Email: james.lee@york.ac.uk

474

475

476 **Acknowledgements**

477 The authors would like to thank BT, in particular Robert Semon, Karen Ahern and Andy
478 Beale for their support in granting access to the BT tower for the measurements and logistical
479 help in setting up the instrumentation. Thanks go to Janet Barlow and Christoforos Halios for
480 provision of the fast the meteorological and boundary layer data at the BT tower. The work
481 was funded through the UK Natural Environment Research Council (NERC) ClearLo
482 project (grant number NE/H00324X/1).

483

484 **References**

485 (1) Tunnicliffe, W. S.; Burge, P. S.; Ayres, J. G., Effect of domestic concentrations of
486 nitrogen dioxide on airway responses to inhaled allergen in asthmatic patients. *Lancet* **1994**,
487 *344*, (8939-4), 1733-1736.

488 (2) Strand, V.; Svartengren, M.; Rak, S.; Barck, C.; Bylin, G., Repeated exposure to an
489 ambient level of NO₂ enhances asthmatic response to a nonsymptomatic allergen dose.
490 *European Respiratory Journal* **1998**, *12*, (1), 6-12.

491 (3) Logan, J. A.; Prather, M. J.; Wofsy, S. C.; McElroy, M. B., Tropospheric Chemistry - A
492 Global Perspective. *J. Geophys. Res.* **1981**, *86*, (NC8), 7210-7254.

493 (4) AQD, Directive 2008/50/EC of the European Parliament and of the Council of 21 May
494 2008 on ambient air quality and cleaner air for Europe. **2008**.

495 (5) Brookes, D. M.; Stedman, J. R.; Kent, A. J.; King, R. J.; Venfield, H. L.; Cooke, S. L.;
496 Lingard, J. J. N.; Vincent, K. J.; Bush, T. J.; Abbott, J., Technical report on UK
497 supplementary assessment under the Air Quality Directive (2008/50/EC), the Air Quality
498 Framework Directive (96/62/EC) and Fourth Daughter Directive (2004/107/EC) for 2011.
499 *Ricardo-AEA report: AEAT/ENV/R/3316* **2012**.

500 (6) Misra, A.; Passant, N. R.; Murrells, T. P.; Thistlethwaite, G.; Pang, Y.; BNorris, J.;
501 Walker, C.; Stewart, R. A.; MacCarthy, J.; Pierce, M., UK emission projections of air quality
502 pollutants to 2030. *AEA Technology report AEA/ENV/R/3337*, **2012**, ([http://uk-
503 air.defra.gov.uk/reports/cat07/1211071420_UEP43_\(2009\)_Projections_Final.pdf](http://uk-air.defra.gov.uk/reports/cat07/1211071420_UEP43_(2009)_Projections_Final.pdf)).

504 (7) Derwent, R. G.; Middleton, D. R.; Field, R. A.; Goldstone, M. E.; Lester, J. N.; Perry,
505 R., Analysis and interpretation of air quality data from an urban roadside location in central
506 London over the period July 1991 to July 1992. *Atmos. Env.* **1995**, *29*, (8), 923-946.

- 507 (8) Sillman, S., The relation between ozone, NO_x and hydrocarbons in urban and polluted
508 rural environments. *Atmos. Env.* **1999**, 33, (12), 1821-1845.
- 509 (9) Carslaw, D. C., Evidence of an increasing NO₂/NO_x emissions ratio from road traffic
510 emissions. *Atmos. Env.* **2005**, 39, (26), 4793-4802.
- 511 (10) Beevers, S. D.; Westmoreland, E.; de Jong, M. C.; Williams, M. L.; Carslaw, D. C.,
512 Trends in NO_x and NO₂ emissions from road traffic in Great Britain. *Atmos. Env.* **2012**, 54,
513 107-116.
- 514 (11) Carslaw, D. C.; Beevers, S. D.; Tate, J. E.; Westmoreland, E. J.; Williams, M. L.,
515 Recent evidence concerning higher NO_x emissions from passenger cars and light duty
516 vehicles. *Atmos. Env.* **2011**, 45, (39), 7053-7063.
- 517 (12) Simon, H.; Allen, D. T.; Wittig, A. E., Fine particulate matter emissions inventories:
518 Comparisons of emissions estimates with observations from recent field programs. *J. Air*
519 *Waste Manage. Assoc.* **2008**, 58, (2), 320-343.
- 520 (13) Han, K. M.; Song, C. H.; Ahn, H. J.; Park, R. S.; Woo, J. H.; Lee, C. K.; Richter, A.;
521 Burrows, J. P.; Kim, J. Y.; Hong, J. H., Investigation of NO_x emissions and NO_x - related
522 chemistry in East Asia using CMAQ-predicted and GOME-derived NO₂ columns. *Atmos.*
523 *Chem. Phys.* **2009**, 9, (3), 1017-1036.
- 524 (14) Ying, Q.; Lu, J.; Allen, P.; Livingstone, P.; Kaduwela, A.; Kleeman, M., Modeling air
525 quality during the California Regional PM₁₀/PM_{2.5} Air Quality Study (CRPAQS) using the
526 UCD/CIT source-oriented air quality model - Part I. Base case model results. *Atmos. Env.*
527 **2008**, 42, (39), 8954-8966.

528 (15) Lee, X.; Massman, W.; Law, B., *Handbook of micrometeorology: a guide for surfact*
529 *flux measurement and analysis* Kluwer Academic Publishers, Dordrecht, The Netherlands:
530 2004.

531 (16) Moore, T. O.; Doughty, D. C.; Marr, L. C., Demonstration of a mobile Flux
532 Laboratory for the Atmospheric Measurement of Emissions (FLAME) to assess emissions
533 inventories. *J. Environ. Monit.* **2009**, *11*, (2), 259-268.

534 (17) Aubinet, M.; Chermanne, B.; Vandenhaute, M.; Longdoz, B.; Yernaux, M.; Laitat, E.,
535 Long term carbon dioxide exchange above a mixed forest in the Belgian Ardennes. *Agric.*
536 *For. Meteorol.* **2001**, *108*, (4), 293-315.

537 (18) Davison, B.; Taipale, R.; Langford, B.; Misztal, P.; Fares, S.; Matteucci, G.; Loreto,
538 F.; Cape, J. N.; Rinne, J.; Hewitt, C. N., Concentrations and fluxes of biogenic volatile
539 organic compounds above a Mediterranean macchia ecosystem in western Italy.
540 *Biogeosciences* **2009**, *6*, (8), 1655-1670.

541 (19) Lee, A.; Schade, G. W.; Holzinger, R.; Goldstein, A. H., A comparison of new
542 measurements of total monoterpene flux with improved measurements of speciated
543 monoterpene flux. *Atmos. Chem. Phys.* **2005**, *5*, 505-513.

544 (20) Karl, T.; Guenther, A.; Lindinger, C.; Jordan, A.; Fall, R.; Lindinger, W., Eddy
545 covariance measurements of oxygenated volatile organic compound fluxes from crop
546 harvesting using a redesigned proton-transfer-reaction mass spectrometer. *J. Geophys. Res.*
547 **2001**, *106*, (D20), 24157-24167.

548 (21) Stella, P.; Loubet, B.; Laville, P.; Lamaud, E.; Cazaunau, M.; Laufs, S.; Bernard, F.;
549 Grosselin, B.; Mascher, N.; Kurtenbach, R.; Mellouki, A.; Kleffmann, J.; Cellier, P.,

550 Comparison of methods for the determination of NO-O₃-NO₂ fluxes and chemical
551 interactions over a bare soil. *Atmos. Meas. Tech.* **2012**, *5*, (6), 1241-1257.

552 (22) Min, K. E.; Pusede, S. E.; Browne, E. C.; LaFranchi, B. W.; Wooldridge, P. J.; Cohen,
553 R. C., Eddy covariance fluxes and vertical concentration gradient measurements of NO and
554 NO₂ over a ponderosa pine ecosystem: observational evidence for within-canopy chemical
555 removal of NO_x. *Atmos. Chem. Phys.* **2014**, *14*, (11), 5495-5512.

556 (23) Geddes, J. A.; Murphy, J. G., Observations of reactive nitrogen oxide fluxes by eddy
557 covariance above two midlatitude North American mixed hardwood forests. *Atmos. Chem.*
558 *Phys.* **2014**, *14*, (6), 2939-2957.

559 (24) Rummel, U.; Ammann, C.; Gut, A.; Meixner, F. X.; Andreae, M. O., Eddy covariance
560 measurements of nitric oxide flux within an Amazonian rain forest. *J. Geophys. Res.* **2002**,
561 *107*, (D20).

562 (25) Honrath, R. E.; Lu, Y.; Peterson, M. C.; Dibb, J. E.; Arsenault, M. A.; Cullen, N. J.;
563 Steffen, K., Vertical fluxes of NO_x, HONO, and HNO₃ above the snowpack at Summit,
564 Greenland. *Atmos. Env.* **2002**, *36*, (15-16), 2629-2640.

565 (26) Bakwin, P. S.; Wofsy, S. C.; Fan, S. M.; Fitzjarrald, D. R., Measurements of NO_x and
566 Noy Concentrations and Fluxes Over Arctic Tundra. *J. Geophys. Res.* **1992**, *97*, (D15),
567 16545-16557.

568 (27) Velasco, E.; Pressley, S.; Allwine, E.; Westberg, H.; Lamb, B., Measurements of CO₂
569 fluxes from the Mexico City urban landscape. *Atmos. Env.* **2005**, *39*, (38), 7433-7446.

570 (28) Vesala, T.; Jarvi, L.; Launiainen, S.; Sogachev, A.; Rannik, U.; Mammarella, I.;
571 Siivola, E.; Keronen, P.; Rinne, J.; Riikonen, A.; Nikinmaa, E., Surface-atmosphere
572 interactions over complex urban terrain in Helsinki, Finland. *Tellus B* **2008**, *60*, (2), 188-199.

573 (29) Crawford, B.; Grimmond, C. S. B.; Christen, A., Five years of carbon dioxide fluxes
574 measurements in a highly vegetated suburban area. *Atmos. Env.* **2011**, *45*, (4), 896-905.

575 (30) Langford, B.; Nemitz, E.; House, E.; Phillips, G. J.; Famulari, D.; Davison, B.;
576 Hopkins, J. R.; Lewis, A. C.; Hewitt, C. N., Fluxes and concentrations of volatile organic
577 compounds above central London, UK. *Atmos. Chem. Phys.* **2010**, *10*, (2), 627-645.

578 (31) Langford, B.; Davison, B.; Nemitz, E.; Hewitt, C. N., Mixing ratios and eddy
579 covariance flux measurements of volatile organic compounds from an urban canopy
580 (Manchester, UK). *Atmos. Chem. Phys.* **2009**, *9*, (6), 1971-1987.

581 (32) Velasco, E.; Lamb, B.; Pressley, S.; Allwine, E.; Westberg, H.; Jobson, B. T.;
582 Alexander, M.; Prazeller, P.; Molina, L.; Molina, M., Flux measurements of volatile organic
583 compounds from an urban landscape. *Geophys. Res. Lett.* **2005**, *32*, (20).

584 (33) Marr, L. C.; Moore, T. O.; Klappmeyer, M. E.; Killar, M. B., Comparison of NO_x
585 Fluxes Measured by Eddy Covariance to Emission Inventories and Land Use. *Environ. Sci.*
586 *Technol.* **2013**, *47*, (4), 1800-1808.

587 (34) Bohnenstengel, S. I.; Belcher, S. E.; Aiken, A.; Allan, J. D.; Allen, G.; Bacak, A.;
588 Bannan, T. J.; Barlow, J. F.; Beddows, D. C. S.; Bloss, W. J.; Booth, A. M.; Chemel, C.;
589 Coceal, O.; Di Marco, C. F.; Dubey, M. K.; Faloon, K. H.; Fleming, Z. L.; Furger, M.; Gietl,
590 J. K.; Graves, R. R.; Green, D. C.; Grimmond, C. S. B.; Halios, C. H.; Hamilton, J. F.;
591 Harrison, R. M.; Heal, M. R.; Heard, D. E.; Helfter, C.; Herndon, S. C.; Holmes, R. E.;
592 Hopkins, J. R.; Jones, A. M.; Kelly, F. J.; Kotthaus, S.; Langford, B.; Lee, J. D.; Leigh, R. J.;
593 Lewis, A. C.; Lidster, R. T.; Lopez-Hilfiker, F. D.; McQuaid, J. B.; Mohr, C.; Monks, P. S.;
594 Nemitz, E.; Ng, N. L.; Percival, C. J.; Prévôt, A. S. H.; Ricketts, H. M. A.; Sokhi, R.; Stone,
595 D.; Thornton, J. A.; Tremper, A. H.; Valach, A. C.; Visser, S.; Whalley, L. K.; Williams, L.

596 R.; Xu, L.; Young, D. E.; Zotter, P., Meteorology, air quality, and health in London: The
597 ClearfLo project. *B. Am. Meteorol. Soc.* **2014**.

598 (35) Helfter, C.; Famulari, D.; Phillips, G. J.; Barlow, J. F.; Wood, C. R.; Grimmond, C. S.
599 B.; Nemitz, E., Controls of carbon dioxide concentrations and fluxes above central London.
600 *Atmos. Chem. Phys.* **2011**, *11*, (5), 1913-1928.

601 (36) Dickerson, R. R.; Delany, A. C.; Wartburg, A. F., Further modification of a
602 commercial NO_x detector for high sensitivity. *Rev. Sci. Instr.* **1984**, *55*, (12), 1995-1998.

603 (37) Lee, J. D.; Moller, S. J.; Read, K. A.; Lewis, A. C.; Mendes, L.; Carpenter, L. J., Year-
604 round measurements of nitrogen oxides and ozone in the tropical North Atlantic marine
605 boundary layer. *J. Geophys. Res.* **2009**, *114*.

606 (38) Pollack, I. B.; Lerner, B. M.; Ryerson, T. B., Evaluation of ultraviolet light-emitting
607 diodes for detection of atmospheric NO₂ by photolysis - chemiluminescence. *J. Atmos. Chem.*
608 **2010**, *65*, (2-3), 111-125.

609 (39) Barlow, J. F.; Dunbar, T. M.; Nemitz, E. G.; Wood, C. R.; Gallagher, M. W.; Davies,
610 F.; O'Connor, E.; Harrison, R. M., Boundary layer dynamics over London, UK, as observed
611 using Doppler lidar during REPARTEE-II. *Atmos. Chem. Phys.* **2011**, *11*, (5), 2111-2125.

612 (40) Foken, T.; Wichura, B., Tools for quality assessment of surface-based flux
613 measurements. *Agric. For. Meteorol.* **1996**, *78*, (1-2), 83-105.

614 (41) Foken, T.; Godecke, M.; Mauder, M.; Mahrt, L.; Amiro, B.; Munger, W., Post-field
615 data quality control, in: Handbook of micrometeorology In Lee, X., Ed. Kluwer Academic
616 Publishers: 2004.

617 (42) Hollinger, D. Y.; Richardson, A. D., Uncertainty in eddy covariance measurements
618 and its application to physiological models. *Tree Physiol.* **2005**, *25*, (7), 873-885.

619 (43) Kormann, R.; Meixner, F. X., An analytical footprint model for non-neutral
620 stratification. *Bound.-Layer Meteorol.* **2001**, *99*, (2), 207-224.

621 (44) Bigi, A.; Harrison, R. M., Analysis of the air pollution climate at a central urban
622 background site. *Atmos. Env.* **2010**, *44*, (16), 2004-2012.

623 (45) Wesely, M. L.; Hicks, B. B., A review of the current status of knowledge on dry
624 deposition. *Atmos. Env.* **2000**, *34*, (12-14), 2261-2282.

625 (46) Carslaw, D. C.; Ropkins, K., openair - An R package for air quality data analysis.
626 *Environmental Modelling & Software* **2012**, *27-28*, 52-61.

627 (47) Bush, T. J.; Tsagatakis, I.; King, K.; Passant, N. R., NAEI UK Emission Mapping
628 Methodology 2006. *AEATY/ENV/R/2696* **2006**, available at:
629 <http://www.naei.org.uk/reoprts.php>.

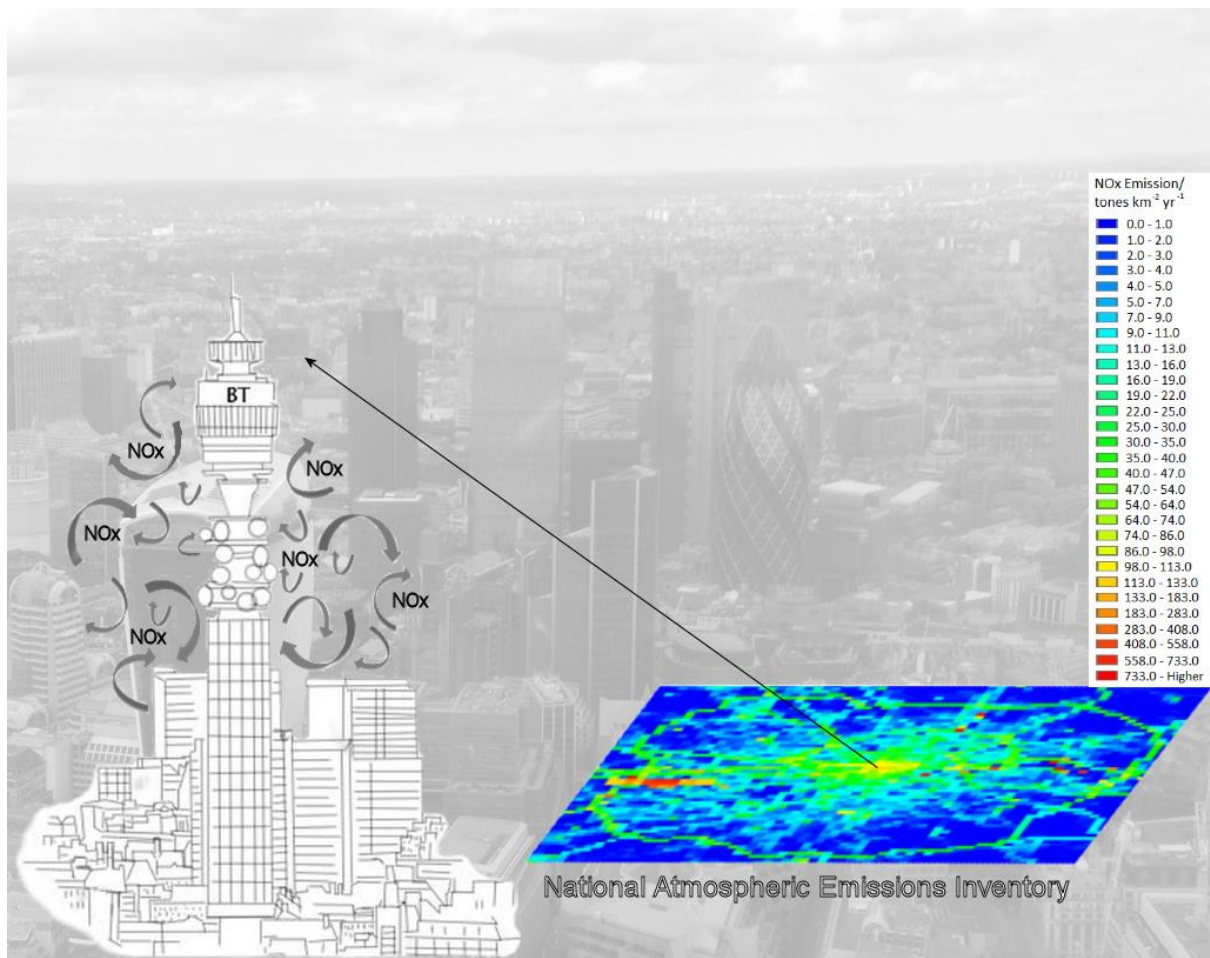
630 (48) Greater London Authority – London Datastore <http://data.london.gov.uk/>.

631 (49) Carslaw, D. C.; Rhys-Tyler, G., New insights from comprehensive on-road
632 measurements of NO_x, NO₂ and NH₃ from vehicle emission remote sensing in London, UK.
633 *Atmos. Env.* **2013**, *81*, 339-347.

634 (50) Carslaw, D. C.; Beevers, S. D., Investigating the potential importance of primary NO₂
635 emissions in a street canyon. *Atmos. Env.* **2004**, *38*, (22), 3585-3594.

636

637



639

640